

# Resolved stellar populations of super-metal-rich star clusters in the bulge of M 31

P. Jablonka<sup>1</sup>, F. Courbin<sup>2</sup>, G. Meylan<sup>3</sup>, A. Sarajedini<sup>4</sup>, T.J. Bridges<sup>5</sup>, and P. Magain<sup>6</sup>

<sup>1</sup> DAEC-URA 8631, Observatoire de Paris-Meudon, Place Jules Janssen, 92195 Meudon, France

<sup>2</sup> Universidad Católica de Chile, Departamento de Astronomía y Astrofísica, Av. Vicuña Mackena 4860, Casilla 306, Santiago 22, Chile

<sup>3</sup> European Southern Observatory, Karl-Schwarzschild-Strasse 2, 85748 Garching, Germany

<sup>4</sup> Astronomy Department, Wesleyan University, Middletown, CT 06459, USA

<sup>5</sup> Anglo-Australian Observatory, P.O. Box 296, Epping, NSW, 1710, Australia

<sup>6</sup> Institut d'Astrophysique, Université de Liège, 5 Avenue de Cointe, 4000 Liège, Belgium

Received 23 February 2000 / Accepted 4 May 2000

**Abstract.** We have applied the MCS image deconvolution algorithm (Magain et al. 1998) to HST/WFPC2 *V*, *I* data of three M 31 bulge globular clusters (G170, G177, and G198) and control fields near each cluster. All three clusters are clearly detected, with an increase in stellar density with decreasing radius from the cluster centers; this is the first time that stars have been resolved in bulge clusters in the inner regions of another galaxy. From the RGB slopes of the clusters and the difference in *I* magnitude between the HB and the top of the RGB, we conclude that these three clusters all have roughly solar metallicity, in agreement with earlier integrated-light spectroscopic measurements. Our data support a picture whereby the M 31 bulge clusters and field stars were born from the same metal-rich gas, early in the galaxy formation.

**Key words:** methods: data analysis – galaxies: formation – galaxies: individual: M 31 – galaxies: spiral – galaxies: star clusters – galaxies: stellar content

## 1. Introduction

Stellar populations are used as tools to probe formation histories in galaxies. The bulge of our Galaxy, together with that of our Local Group galaxy companion M 31, have colors, metallicities, and kinematics which are typical of early type spiral bulges. Although our knowledge about bulges has improved during the last decade, little is known about their formation and evolution, especially in connection with the other components of galaxies (Freeman 1993). There is, however, recent evidence that bulges originate, on rather short time scales, during the very first phases of galaxy formation. For example, in our Galaxy, the analysis of Color-Magnitude Diagrams (CMDs) of star clusters located within five degrees of the Galactic center has revealed a metallicity distribution similar to that of the surrounding Galactic field stars (Barbuy et al. 1998). In addition, the metal-rich

bulge clusters have been demonstrated to have the same age as the inner-halo metal-rich old globular cluster 47 Tucanae (Ortolani et al. 1995).

The globular cluster system of M 31, which is about twice as rich as the Galactic one, is among the most studied cluster systems in external galaxies (Harris 1991). However, our knowledge comes mainly from the photometric and/or spectroscopic integrated properties of these clusters. A few pioneering attempts have been made to obtain cluster CMDs from the ground, but even with good seeing at the CFHT, Heasley et al. (1988) and Christian & Heasley (1991) were only able to reach the upper part of the red giant branch, without reaching the horizontal branches of G1 and G219, two of the brightest M 31 clusters.

With the advent of the Hubble Space Telescope (HST), the situation has changed. The CMDs of 10 globular clusters in M 31 have been published, reaching about one magnitude below the horizontal branch (Fusi-Peccì et al. 1996, Ajhar et al. 1996, Rich et al. 1996, Holland et al. 1997). These clusters are mainly located in the halo of M 31, where contamination from foreground stars and the M 31 stellar disk is minimized. The closest to the center are G108 (with  $[Fe/H] = -0.94$ ) and G280 (with  $[Fe/H] = -0.4$ ), located at  $19.2' = 4.81$  kpc and  $18.4' = 4.59$  kpc from the M 31 center, respectively.

Recently, Jablonka et al. (1992, 1998) obtained integrated spectrophotometric observations for a sample of globular clusters in the bulge of M 31, looking for possible extreme cases of metal enrichment, and consequently naturally investigated the inner regions of M 31. The two clusters G170 and G177 belong to their sample. G177 exhibits metallic absorption features which are as strong as those characterizing the central regions of elliptical galaxies; with its higher-than-solar metallicity, this cluster clearly challenged the conventional view of old globular clusters as metal-poor objects, although such metal-rich clusters seem to be rare. Another cluster, G198, as super-metal rich as G177 and at about the same distance from the M 31 center, had been identified by Huchra et al. (1991) in an independent spectroscopic analysis. G170, located slightly further away has about a solar metallicity.

*Send offprint requests to:* P. Jablonka

*Correspondence to:* pascale.jablonka@obspm.fr

As a first attempt to learn more about the outstanding properties of extremely metal-rich globular clusters, we applied for deep imaging observations with the HST, taking advantage of the high spatial resolution and red sensitivity of the Planetary Camera of WFPC2, in order to build the CMDs of these three M 31 bulge clusters, all of them located within about six arcmin from the center of this galaxy. These cluster data, so far the closest to the center of M 31, allow insight into the questions of metallicities, age and link between bulge field and cluster stellar populations. Given their central location and consequently their very high stellar density, they challenge the best observational capabilities. G170, being slightly further away from the center, is surrounded by a lower density of field stars than the other two clusters, and was meant to be a relative calibrator. A fourth cluster, G1, has been observed during the same program; its properties, viz. CMD, structural parameters, dynamical mass estimate, and M/L ratio, will be addressed in another paper (Meylan et al. 2000).

The structure of this paper is as follows: Sect. 2 presents the observations and data reduction; Sect. 3 describes the image deconvolution technique used; Sect. 4 analyses and discusses the results, while Sect. 5 summarizes the highlights of this study.

## 2. Observations

We obtained HST WFPC2 images with the F555W ( $V$ ) and F814W ( $I$ ) filters, during Cycles 5 and 6 (Program IDs = 5907 and 6477). Our targets were field and cluster stars around three metal-rich star clusters G170, G177, and G198 in the bulge of M 31 (Jablonka et al. 1992; Huchra et al. 1991). The two fields around the star clusters G170 and G177 are located South-West along the major axis of M 31, respectively at 6.1' and 3.2' from the galaxy nucleus; the third field, around the cluster G198, is located North-East along the major axis at 3.7' from the galaxy nucleus (Huchra et al. 1991; Hodge 1981). Adopting  $1' = 250$  pc (Rich & Mighell 1995), these angular separations correspond to projected distances of about 1.55, 0.80, and 0.92 kpc, respectively. These distances are summarized in Columns 2 and 3 of Table 1. Columns 4 and 5 of the same table provide the  $V$  magnitude and  $B - V$  color of each cluster, from Battistini et al. (1987). Fig. 1 in Jablonka et al. (1999) gives the location of our fields.

Fig. 1 displays, on the left, for each of the three clusters, an area of  $64 \times 64$  pixels from the original PC frames, centered on the clusters. With the PC pixel size of  $0.045''/\text{pix}$ , this corresponds to squares of  $2.88''$  in size. Although resolved, all three clusters appear extremely compact, with very steep surface brightness profiles and extremely crowded and bright cores. Since all images are slightly saturated in the core of the clusters this prevents the determination of the cluster structural parameters. In any case, these three clusters are extremely concentrated, being probably close to core collapse.

Our data represent one of the highest resolution images obtained so far of the innermost parts of M 31 for either cluster or field stars. While the high spatial resolution of the HST is necessary when studying crowded fields, its unfortunate under-

sampling limits the effectiveness of the instrument in actually resolving blends of stars. The consequences of various samplings on the study of crowded stellar fields is investigated by Renzini (1998), who shows by clear physical considerations that the main limiting factor is the number of stars per resolution element. For whatever available spatial resolution provided by a given telescope, the sampling of the images as determined by the CCD still sets the number of degrees of freedom (pixels), as compared with the number of unknowns (star intensities).

In the center of M 31, the number of unknowns is close to that of the available degrees of freedom, making it difficult to obtain the photometry of individual stars. In this context, the photometry is affected not only by the photon noise, but also by systematic errors. Systematics translate into biased photometry and may even depend on the algorithm used. For example, the way the sky subtraction is performed influences significantly the results in images where basically no single pixel provides an accurate estimate of the sky brightness. An algorithm which treats the sky background globally (i.e., the sky background is an image) will usually not produce the same photometry as an algorithm which computes a local sky value. The sky level will usually be *systematically* over- or under-estimated, hence leading to biased photometry (such an effect, is of course best seen in faint stars, close to the sky level). Another source of systematic errors comes from the way heavy blends are handled by the photometry software: an algorithm which does not “see” very blended stars will tend to overestimate the flux of multiple point sources identified as one single source. While correcting for the net effect of such systematics is extremely difficult, one may still be able to quantify their magnitude. For this purpose, we performed our analysis with two very different algorithms: the ALLFRAME procedure developed by P. Stetson (1994), and the “MCS image deconvolution algorithm” developed by Magain et al. (1998).

Both ALLFRAME and MCS have been run on the  $64 \times 64$ -pixel ( $2.88'' \times 2.88''$ ) sub-areas of the original PC frames. The small size of these images has been chosen to minimize the CPU consumption of the MCS method. The clusters are centered and fully included in these subimages. Reference sub-areas in the same PC frames, hereafter called control fields, with similar  $64 \times 64$ -pixel size, have been chosen at about  $10''$  away from the clusters, far enough to ensure that no cluster star would intervene, though not too far away, so that the conditions of analysis remain the same. The directions between cluster fields and control fields are also chosen to minimize any effect induced by the strong gradient of the bulge stellar field. Table 1 gathers the coordinates of the cluster and control fields in pixel units of the PC frames. As ALLFRAME is now widely known and since our use of it is already described in Jablonka et al. (1999), we mainly focus in the following section on the description of our use of the MCS deconvolution algorithm.

## 3. Image deconvolution

The MCS deconvolution algorithm is applied to the combined  $V$  and  $I$  frames, viz., 4 frames in each of the  $V$ - and  $I$ -bands. Fig. 1

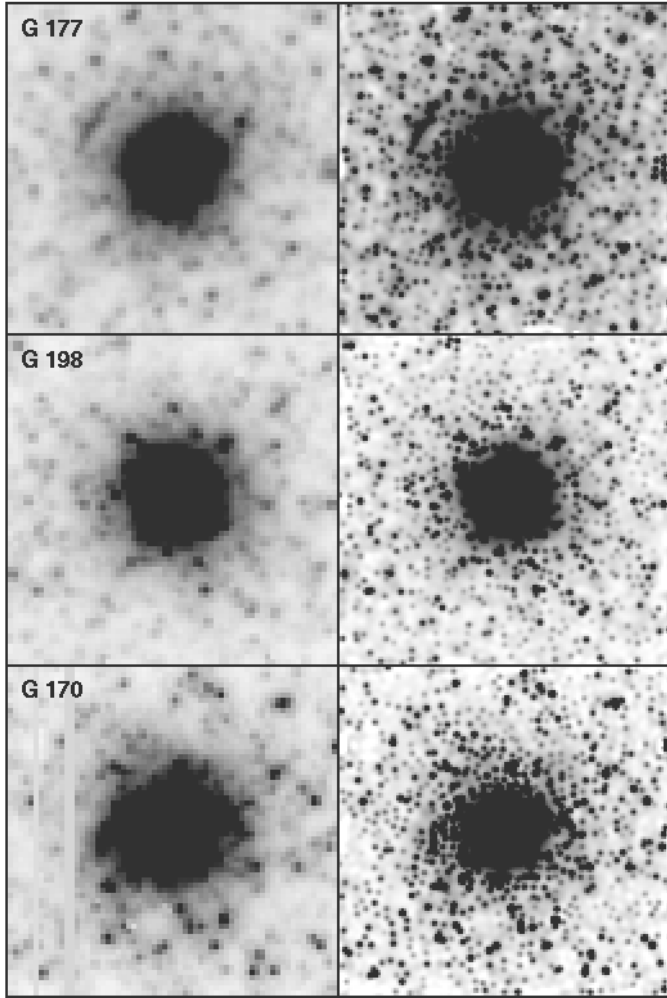


**Fig. 1.** Left: These three panels display  $64 \times 64$  pixels ( $2.88'' \times 2.88''$ ) area from the original F814W =  $I$  PC frames, centered on the three M 31 star clusters G177, G198, and G170. Right: these three panels display the corresponding results of the MCS deconvolution algorithm.

(left) displays for each cluster the  $64 \times 64$ -pixel area centered on the cluster, from one of the the  $I$ -band images, after the classical HST pipeline data reduction procedure. Fig. 1 (right) displays the resulting image after the MCS deconvolution.

The PSF is known to be variable across the WFPC2 field with a scale of about  $30''$ . Consequently, the PSF can be safely assumed to be constant over each of our small  $64 \times 64$ -pixel areas, but different PSFs were computed for each cluster and each control field. These PSFs were obtained from the grid of numerical PSF estimates made available to us by P. Stetson from the Cepheid Key Project. The F555W and F814W instrumental magnitudes were converted to Johnson-Cousins  $V$  and  $I$  magnitudes, using the zero points in Holtzman et al. (1995) and the color terms given by Hughes et al. (1998) for their Key Project WFPC2 data. No aperture correction was applied. The resulting color transformation equations are:

$$V = V_{MCS} - 0.045(V - I) + 0.027(V - I)^2 + 21.725 + 2.5 \log(1.987)$$

$$I = I_{MCS} - 0.067(V - I) + 0.025(V - I)^2 + 20.839 + 2.5 \log(1.987)$$

Our cluster and control fields fall close to four PSF estimates on the PSF grid, so that we were able to compute the final PSFs used for the deconvolution on a grid of pixels a factor of two smaller than the original pixel size; this is similar to the “drizzling” procedure used to over-sample images, using various dithered frames of the same field (Fruchter & Hook 1998). The final pixel size adopted to sample the deconvolved images is then  $0.0225''$ . Adopting this smaller pixel size is essential when deconvolving slightly under-sampled data as those from WFPC2. We can then improve the spatial resolution beyond the limits in principle imposed by the pixel size in the original data frame and reach with 2 (smaller) pixels a final resolution equal to  $0.045''$  FWHM, without violating the sampling theorem.

The deconvolved numerical images are decomposed into a sum of point sources and background, where the background includes, in the present application, not only the sky background and all possible extended sources, but also the diffuse light from the stellar population still unresolved in spite of the use of the HST. The user of the MCS deconvolution algorithm has to decide how many point sources are present in the deconvolved image: in the present crowded fields, we may miss many of the faint and/or overly blended stars. While the stars missed are obviously not measured as point sources, because they are not present in the point-source part of the deconvolved image, they are nevertheless still present in the background component of the image. Light pollution of the stars actually identified as point sources is therefore minimized.

Several consecutive deconvolutions are run in order to identify as many stars as possible during this iterative process. The number of point sources to be involved in the deconvolution can be objectively defined by checking the quality of the residual map (RM), which is the difference between the original data frames and the deconvolved images (re-convolved with the PSF), in units of photon noise (e.g., Courbin et al. 1998). A good deconvolution, i.e., with the optimum number of point sources involved in the fit, should leave a flat RM with mean value of  $1\sigma$ . Missing one or several stars results in significant residuals, above the critical value of 1. Adding too many stars results in over-fitting of the data and local residuals below 1. We therefore always choose the minimum number of stars leading to a statistically acceptable RM. Such a criterion, which works successfully when data are correctly sampled, is more difficult to apply here. This is true for all 3 clusters, and it is clear that we miss in all cases a significant fraction of the stars, especially close to the cluster centers. One additional and reliable criterion we apply to select the stars to construct our CMDs is to stipulate that the detection of a star is genuine only if it is present in both the  $V$  and  $I$  images and if its position is the same in the two bands, within an error box of 0.25 pixels (in the original data frames).

Importantly, knowing the PSF on a grid of pixels smaller than in the original data frames minimizes the limitation related to the larger pixel size of the HST. The number of degrees of

**Table 1.** Cluster Information

| Cluster Name | Distance<br>[arcmin] | Distance<br>[kpc] | $V$<br>[mag] | $B - V$<br>[mag] | Cluster Field<br>(x1:x2; y1:y2) | Control Field<br>(x1:x2; y1:y2) |
|--------------|----------------------|-------------------|--------------|------------------|---------------------------------|---------------------------------|
| G177         | 3.2                  | 0.80              | 15.91        | 1.31             | 386:449; 415:478                | 224:287; 510:573                |
| G198         | 3.7                  | 0.92              | 15.98        | 1.24             | 322:385; 332:395                | 602:665; 405:468                |
| G170         | 6.1                  | 1.55              | 16.45        | 1.23             | 524:587; 352:415                | 278:341; 320:383                |

freedom per unknown is still fixed by the physical pixel size of the detector, but we are able to resolve closer blends with the deconvolution algorithm than with ALLFRAME. The typical minimum distance between two point sources of similar brightness is about 0.3 pixels (in the original data frame) with the deconvolution, while ALLFRAME rejects all blends closer than about 0.7 pixels, equivalent to 0.37 times the FWHM of the PSF. The systematics arising from strong blends (see Sect. 2) should therefore be less severe in the MCS deconvolution photometry than in the profile fitting photometry. However, the sky background (which also included unresolved stars) cannot be modelled properly using our data. In order to test the systematic errors which may be introduced by unsecure sky background determination, we ran the deconvolution several times, with different initial parameters and smoothing strengths (see MCS). We noted that the magnitudes measured for the faintest stars can be affected by offsets of up to 0.3 magnitudes in both bands (peak to peak variations), between two consecutive deconvolutions using different parameters. We therefore estimate that our results are affected by *systematic errors* (i.e., all stars systematically too bright or too faint) of about 0.07 magnitudes ( $1\sigma$  error, calculated as 0.3 divided by 2 (peak-to-peak total spread and divided by 3, to translate 3 sigma errors into 1 sigma errors) in both bands. This leads to shifts in color of 0.1 mag ( $1\sigma$ ). The  $1\sigma$  error on the positions of the sequences in our CMDs, due to systematic errors alone are therefore of the order of 0.07 mag in ordinate and 0.1 mag in color.

## 4. Results and discussion

### 4.1. Star counts

Figs. 2 present our results from ALLFRAME and the MCS deconvolution. We plot the number of detected stars per square arcsec as a function of the radius, calculated outwards from the centers of the clusters or of the reference fields. For the clusters, we neglect all points within  $0.55''$  of the cluster centers, where the crowding is too high to allow any reliable results for either method of analysis. We also apply magnitude cuts and keep only stars with  $V \leq 26.5$  mag and  $I \leq 24.5$  mag. These cuts are necessary if one wants to properly compare the field and the cluster stars which is one of the main aims of the present work. Indeed, the density is higher in the cluster regions and thus prevents us going as deep as in the field. However, only a few stars are excluded by this criterion. These magnitude cuts, for both ALLFRAME and the MCS deconvolution, correspond to maximum internal errors (photon noise only) of 0.2 mag. The total

errors on the photometry of the brighter stars are significantly smaller (0.01 mag for the brightest).

In Fig. 2, we expect to see the following two effects. (i) Detection of the clusters: the star counts for the cluster fields should decrease as a function of increasing radius, as the successive rings contain fewer and fewer cluster stars, mixed with some field stars. (ii) Detection of the M 31 field gradient: there should be no detectable gradient in star counts *within* each small control field; however the gradient should be observable from one field to the other, i.e., when considering the three different cluster regions, G177, G198 and G170 in increasing distance to the M 31 center (Table 1).

#### 4.1.1. Detection of the clusters

The cluster G170 is very clearly detected. The star counts provided by ALLFRAME are significantly different in the cluster and control fields (Fig. 2 lower left panel) and agree closely with those provided by MCS deconvolution (Fig. 2 lower right panel). There is a clear increase in stellar density at the vicinity of the cluster, although with more stars detected with the MCS deconvolution. With decreasing radius, ALLFRAME star counts increase from 35 to 70 stars/arcsec<sup>2</sup>, while MCS deconvolution star counts increase from 40 to 95 stars/arcsec<sup>2</sup>. At the distance of G170, the density of bulge field stars is low enough so that everywhere in the cluster field the density of detected stars is higher than in the control field. If one consider the MCS counts, the control field contains about 30 stars per square arcsec. The outskirts of G170 have a stellar density of  $\sim 50$  stars per square arcsec, which means that there are nearly as many cluster stars as field stars. From  $0.75''$  inwards, the number of stars from the cluster represent  $2/3$  of the total stellar population.

In the case of G177 and G198, the situation is less favorable. With ALLFRAME, the star counts of the cluster fields remain compatible with those of the control fields (Fig. 2 upper and middle left panels). With the MCS deconvolution (Fig. 2 upper and middle right panels), the star counts increase within  $1''$ . There, the cluster stars represent about half of the total stellar population. This means that, although quite conspicuous on the original frames, stars in G177 and in G198 were not detected by the reduction procedure which employed ALLFRAME and are marginally detected by the MCS deconvolution. The ability of softwares to find stars depends very much on how it can cope with poor sampling and on how well it performs the background/point source separation, especially in crowded environments. We do not detect the presence of G177 and G198 with ALLFRAME, as the confusion limit has been reached for this

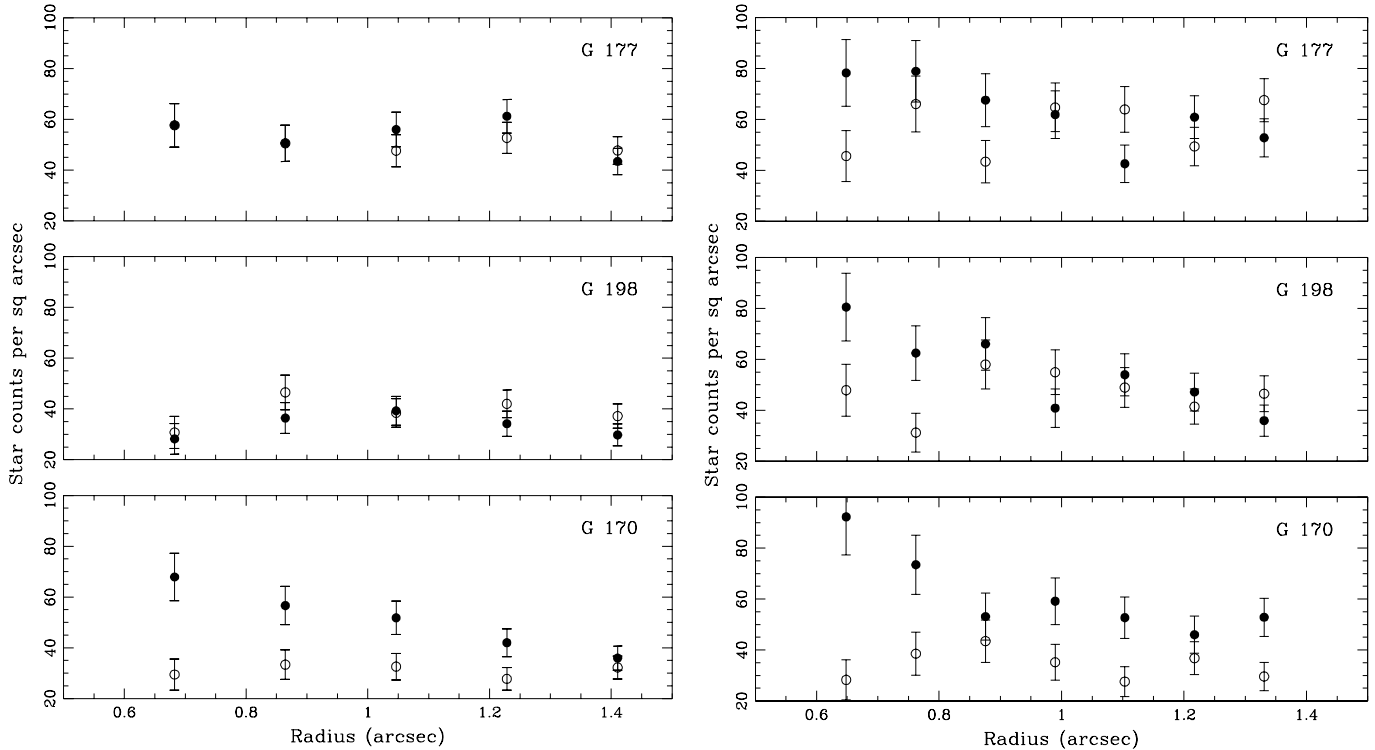


**Fig. 2.** Radial star counts for all stars detected with ALLFRAME (left panel), and with the MCS deconvolution (right panel), for each of our three clusters and their control fields. The filled circles refer to the cluster counts, while the open circles refer to the control fields.

technique; thus the number of detected stars may even fall below the background value, and stays basically at the same level, independently of the distance from the cluster center.

#### 4.1.2. Detection of the M 31 field gradient

This gradient can be detected in the control fields and in the outermost points of the cluster fields when considering the mean level of star counts. From both ALLFRAME and MCS deconvolution star counts, the average density of field stars in clusters and control fields is about 30 stars/arcsec<sup>2</sup> around G170, about 40 stars/arcsec<sup>2</sup> around G198, and 55 stars/arcsec<sup>2</sup> around G177. In both methods of analysis, the mean density of field stars increases significantly when considering the fields close to G170, G198, and G177, respectively, as expected from their locations closer and closer to the galaxy center.

From these considerations, given the success of the MCS deconvolution in detecting the cluster stars of G177 and G198, we discuss below only the photometry resulting from this procedure, in the form of CMDs for each of the three clusters and control fields.

#### 4.2. The photometry

Fig. 3 displays the ( $I$  vs.  $V - I$ ) CMDs resulting from the MCS deconvolution, for both the control (left) and cluster (right) fields. In all six panels, we clearly see the field and cluster red giant branches (RGB). The CMDs extend to slightly below the

level of the horizontal branch (HB) at  $I = 24.35$ , though we do not have many HB stars due to our general completeness limit (see Jablonka et al. 1999) and to the poor statistics in such small regions.

In the CMDs shown in the right panel of Fig. 3, the RGB sequences of the clusters G177 and G198 are slightly bluer by  $\sim 0.15$  mag than those of their respective control fields (left panels). In addition, the CMDs between the clusters also exhibit a comparable variation in their mean colors. This effect is due to the increase in density from the fields to the clusters or from one mean location to another closer to the M 31 center and is especially visible between the G170 location and the others. The effect of crowding leads to blends of stars as already discussed by means of artificial star experiments in Jablonka et al. (1999). As illustrated in Fig. 4, while the faint and bright ends of the luminosity functions are not modified, when moving to higher star densities, the bulk of stars are shifted towards higher luminosities by blends of intermediate luminosity stars. Since we observe intrinsically red stellar populations, confusion is more pronounced in  $V$  than in  $I$ , so that more unresolved blends are faced in  $V$ , due to shallower contrast (i.e., dynamic range), hence leading to bluer colors. As the brightest end of the magnitude distribution is not affected, the location of the reddest part of the RGB is safe and allows analysis of age and abundance. We estimate that these systematic effects may translate into errors as large as 0.3 mag in  $V - I$  at  $I \sim 24.5$  mag (see Sect. 3), but should not be larger than 0.1 mag at  $I \sim 22\text{--}22.5$  mag, at a  $3\sigma$  level.

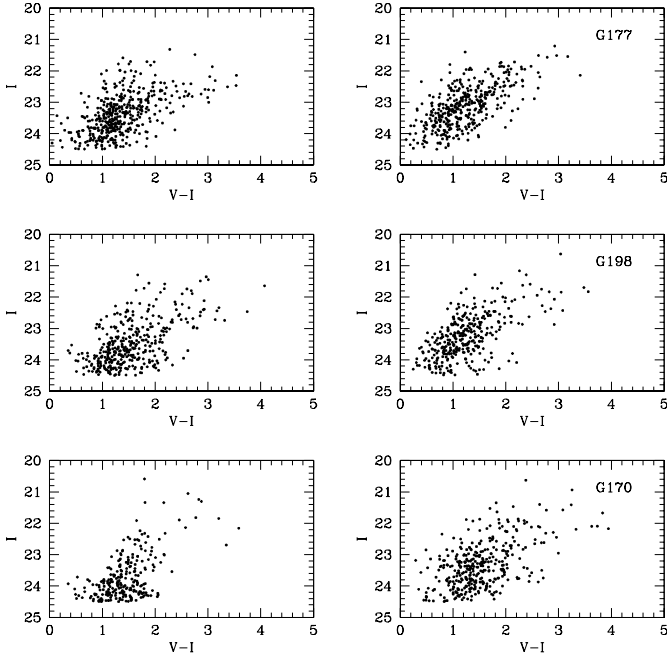


**Fig. 3.** CMDs for all three control (left) and cluster (right) fields. The  $1-\sigma$  errors in  $I$  are of the order of 0.15 mag between 23.5 and 24.5 mag, 0.02 mag between 22.5 and 23.5 mag, 0.005 mag between 21.5 and 22.5 mag. The  $1-\sigma$  errors in  $V$  are of the order of 0.2 mag between 25.5 and 26.5 mag, 0.07 mag between 24.5 and 25.5 mag, 0.01 mag between 24.5 and 23.5 mag.

Following the approach of Ortolani et al. (1991), we derive the RGB slopes of our clusters in  $I$  and  $V$  (see Table 2). We also indicate the differences in  $I$  magnitude between the Horizontal Branch (HB) level and the top of the RGB (the brightest stars) which is a complementary indicator of metallicity (Barbuy et al. 1997). For G170 all stars in the 64x64 pixels frame are included, while for G177 and G198, only stars within a  $1''$  radius are used in the calculation, the region where the presence of cluster stars is unambiguous. The horizontal branch level for the clusters has been taken to be equal to that of the field. Fusi Pecci et al. (1996) give  $M_V^{HB} \propto 0.13 [\text{Fe}/\text{H}]$ . In our case, even if the clusters were less metallic than the field, it would be hardly by more than 0.6 dex, otherwise we would detect brighter red stars than we do; thus the change in magnitude for the HB stars going from the field to the clusters, or even from one cluster to another would be smaller than our photometric precision. The mean magnitude of HB stars at  $I \sim 24.35$  mag has been measured from the luminosity function of the entire PC frame around G170. For comparison and ranking of the three M 31 clusters, we indicate the values derived for NGC 6528 and NGC 6553, bulge clusters in our Galaxy, both at  $[Z/Z_\odot]=0.0$  (Ortolani et al. 1995; Barbuy et al. 1999) and for the Galactic thick disk cluster 47 Tuc. The number of stars on the red extension of the giant branch of G177 ( $V-I \geq 2.5$  mag) in the inner  $1''$  radius is too low to give reliable slopes or magnitude differences. Indeed, given the small areas considered, poor statistics prevents us from measuring the RGB slope for G177. All three clusters have previous spectroscopic determinations of their global metal abundance,  $[Z/Z_\odot] = 0$  and

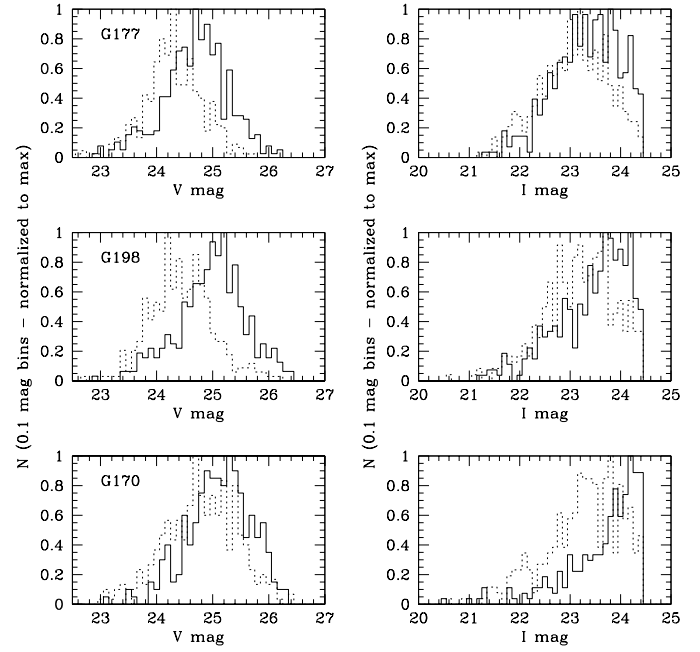


**Fig. 4.**  $V$  (left) and  $I$  (right) luminosity functions for control and cluster fields. Solid lines give the field luminosity functions and the dotted lines the cluster luminosity functions.

**Table 2.** RGB slopes and magnitudes

| Cluster  | $[Z/Z_\odot]$ | $\Delta I / \Delta(V - I)$ | $\Delta V / \Delta(V - I)$ | $\Delta I_{HB}^{RGB}$ |
|----------|---------------|----------------------------|----------------------------|-----------------------|
| 47 Tuc   | -0.4          | $-0.24 \pm 0.07$           | $0.77 \pm 0.07$            | 3.46                  |
| NGC 6528 | 0.0           | $-0.06 \pm 0.07$           | $0.82 \pm 0.07$            | 2.8                   |
| NGC 6553 | 0.0           | $-0.02 \pm 0.10$           | $0.92 \pm 0.2$             | 2.7                   |
| G170     | $\sim 0.0$    | $+0.01 \pm 0.08$           | $1.00 \pm 0.08$            | 3.                    |
| G177     | $\sim 0.0$    | -                          | -                          | 2.8                   |
| G198     | $\sim 0.0$    | $+0.01 \pm 0.07$           | $1.00 \pm 0.10$            | 3.1                   |

0.3, for G170 and G177 and  $[\text{Fe}/\text{H}] = 0.09$  for G198 (Jablonka et al. 1992, Huchra et al. 1991). The present estimates, although crude, are in very good agreement, as they rank the clusters at the level of NGC 6553 and NGC 6528. This gives us enough confidence in our photometry to pursue the comparison between the cluster and field stellar population.

From the various CMDs in Fig. 3, and given our error bars and systematic biases discussed above due to image crowding, we are led to conclude that there is no significant difference between the cluster and the mean field stellar populations; the clusters are indeed in the M 31 bulge and are not seen in projection. Our data indicate a formation of the M 31 bulge clusters from the same material as that of the field stars, at an early epoch in the formation of M 31.

## 5. Conclusions

We have applied the MCS deconvolution algorithm to three M 31 bulge globular clusters. This deconvolution appears as a very efficient method in such extremely dense regions, but still rather demanding in terms of computing time, so we have been

limited to small regions. However, our initial results are already very promising. Our radial star counts for the cluster and control fields clearly show that we have resolved the clusters: this is the first time that cluster stars have been resolved in the bulge of another galaxy so close to the center.

From the deconvolved photometry, we clearly see the cluster red giant branches, though we do not detect their horizontal branches. Taking into account systematic biases introduced by crowding, there are no significant differences between the CMDs for the three clusters. Moreover, there is no apparent difference between the cluster and their respective control field CMDs. From the RGB slopes and the difference in  $I$  magnitude between the HB and RGB, all three clusters have roughly solar metallicity, making them similar to NGC 6528 or NGC 6553 in our Galaxy; by inference, the same is true of the mean field population.

We thus conclude that the M 31 bulge clusters and field stars originate from the same material. They are representative of old, metal-rich populations. Similar results have been found in our Galaxy, where it becomes more and more apparent that the metallicity distributions of field stars and globular clusters in the bulge are identical (Ortolani et al. 1995; Barbuy et al. 1998). From a detailed study of the element ratios for two stars in NGC 6553, Barbuy et al. (1999) conclude that the Galactic bulge underwent rapid star formation and chemical enrichment. Certainly our work corroborates this view. Bulges appear to be old, metal-rich systems, similar in many respects to elliptical galaxies. There is mounting evidence that most stars in ellipticals and bulges formed at high redshift  $z_f > 3$  (see review by Renzini & Cimatti 1999).

Unfortunately, we have pushed HST to its limits, and M 31 seems to be the furthest galaxy for which we can use HST in this way. Higher spatial resolution studies of bulge populations in M 31 and more distant galaxies awaits adaptive optics on 8–10m ground-based telescopes, and eventually the NGST.

*Acknowledgements.* We would like to thank Peter Stetson for kindly sharing with us the Cepheid Key Project PSFs, and for his support with ALLFRAME. Ata Sarajedini was supported by the National Aeronautics and Space Administration (NASA) grants HF-01077.01-94A,

GO-05907.01-94A, and GO-06477.02-95A from the Space Telescope Science Institute, which is operated by the Association of Universities for Research in Astronomy, Inc., under NASA contract NAS5-26555. Frédéric Courbin acknowledges financial support through Chilean grant FONDECYT/3990024 and additional funding from the European Southern Observatory.

## References

- Ajhar E.A., Grillmair C.J., Lauer T.R., et al., 1996, AJ 111, 2293  
 Barbuy B., Ortolani S. Bica E., 1997, A&AS 122, 483  
 Barbuy B., Bica E., Ortolani S., 1998, A&A 333, 117  
 Barbuy B., Renzini A., Ortolani S., Bica E., Guarnieri M.D., 1999, A&A 341, 539  
 Battistini P., Bònoli F., Braccési A., et al., 1987, A&AS 67, 447  
 Christian C.A., Heasley J.N., 1991, AJ 101, 848  
 Courbin, F., Lidman C., Frye B., et al. 1998, ApJ 499, L119  
 Freeman K.C., 1993, in: Galactic Bulges, IAU symp. 153, p. 263  
 Fruchter A.S., Hook R.N. 1998, astro-ph 9808087  
 Fusi-Peccì F, Buonanno R., Cacciari C., et al., 1996, AJ 112, 1461  
 Harris W.E., 1991, ARA&A 29, 543  
 Heasley J.N, C.A, Friel E.D., Janes K.A., 1988, AJ 94, 1312  
 Hodge P.W., 1981, Atlas of the Andromeda Galaxy, University of Washington Press  
 Holland S., Fahlman G.G., Richer H.B., 1997, AJ 114, 1488  
 Holtzman, J.A., Burrows C.J., Casertano S., et al., 1995, PASP 107, 1065  
 Huchra J., Brodie J., Kent S., 1991, 370, 495  
 Hughes S.M.G., Han M., Hoessel J. et al., 1998, ApJ 501, 32  
 Jablonka P., Alloin D., Bica E., 1992, A&A 260, 97  
 Jablonka P., Bica E., Bonatto C., et al., 1998, A&A 335, 867  
 Jablonka P., Bridges T.J., Sarajedini A., et al., 1999, ApJ 518, 627  
 Kauffmann G., White S.D.M., Guiderdoni B., 1993, MNRAS 264, 201  
 Magain P., Courbin F., Sohy S., 1998, ApJ 494, 472  
 Meylan G., Sarajedini A., Jablonka P., 2000, in preparation  
 Ortolani S., Barbuy B., Bica E., 1991, A&A 249, L31  
 Ortolani S., Renzini A., Gilmozzi R., et al., 1995, Nat 377, 701  
 Renzini A., 1998, ApJ 115, 2459  
 Renzini A., Cimatti A. 1999, astro-ph 9910162  
 Rich R.M., Mighell K.J., 1995, ApJ 439, 145  
 Rich R.M., Kenneth J., Freedman W.L., Neill J.D., 1996, AJ 111, 768  
 Stetson P., 1994, PASP 106, 250